Hindawi
Bioinorganic Chemistry and Applications
Volume 2020, Article ID 2901439, 14 pages
https://doi.org/10.1155/2020/2901439

Research Article

Dynamic and Static Nature of Br_4 σ(4c–6e) and Se_2Br_5 σ(7c–10e) in the Selenanthrene System and Related Species Elucidated by QTAIM Dual Functional Analysis with QC Calculations

Satoko Hayashi, Taro Nishide, and Waro Nakanishi

Faculty of Systems Engineering, Wakayama University, 930 Sakaedani, Wakayama 640-8510, Japan

Correspondence should be addressed to Satoko Hayashi; hayashi3@sys.wakayama-u.ac.jp and Waro Nakanishi; nakanisi@sys.wakayama-u.ac.jp

Received 22 January 2019; Revised 15 June 2019; Accepted 19 November 2019; Published 24 July 2020

Academic Editor: Claudio Pettinari

The nature of Br_4 σ(4c–6e) of the ^{B}Br-$*$-^{A}Br-$*$-^{A}Br-$*$-^{B}Br form is elucidated for $SeC_{12}H_8$(Br)Se**Br---Br-Br---Br**Se(Br)$C_{12}H_8$Se, the selenanthrene system, and the models with QTAIM dual functional analysis (QTAIM-DFA). Asterisks ($*$) are employed to emphasize the existence of bond critical points on the interactions in question. Data from the fully optimized structure correspond to the static nature of interactions. In our treatment, data from the perturbed structures, around the fully optimized structure, are employed for the analysis, in addition to those from the fully optimized one, which represent the dynamic nature of interactions. The ^{A}Br-$*$-^{A}Br and ^{A}Br-$*$-^{B}Br interactions are predicted to have the CT-TBP (trigonal bipyramidal adduct formation through charge transfer) nature and the typical hydrogen bond nature, respectively. The nature of Se_2Br_5 σ(7c–10e) is also clarified typically, employing an anionic model of [**Br-Se**(C_4H_4Se)-**Br---Br---Br-Se**(C_4H_4Se)-**Br**]$^{-}$, the 1,4-diselenin system, rather than ($BrSeC_{12}H_8$)**Br---Se---Br-Br---Br-Se**($C_{12}H_8$Se)-**Br**, the selenanthrene system.

1. Introduction

We have been much interested in the behavior of the linear interactions of the σ-type, higher than σ(3c–4e: three center-four electron interactions) [1–6], constructed by the atoms of heavier main group elements. We proposed to call such linear interactions the extended hypervalent interactions, σ(*m*c–*n*e: $4 \le m$; $m < n < 2m$), after the hypervalent σ(3c–4e). The linear alignments of four chalcogen atoms were first demonstrated in the naphthalene system, bis[8-(phenylchalcogenyl)naphthyl]-1,1′-dichalcogenides [**I**: 1-(8-Ph^{B}E$C_{10}H_6$)^{A}E-^{A}E($C_{10}H_6$^{B}EPh-8′)-1′ (^{A}E, ^{B}E = S and Se)] [7–12]. It was achieved through the preparation and the structural determination by the X-ray crystallographic analysis. The linear ^{B}E---^{A}E-^{A}E---^{B}E interactions in **I** are proposed to be analysed as the $^{A}E_2{}^{B}E_2$ σ(4c–6e) model not by the double $^{A}E^{B}E_2$ σ(3c–4e) model. $^{A}E_2{}^{B}E_2$ σ(4c–6e) in **I** is characterized by the CT interaction of the $n_p(^{B}E) \longrightarrow \sigma*(^{A}E\text{–}^{A}E) \leftarrow n_p(^{B}E)$ form [8, 10–12], where $n_p(^{B}E)$ stands for the p-type nonbonding orbitals of ^{B}E and $\sigma*(^{A}E\text{-}^{A}E)$ are the $\sigma*$ orbitals of ^{A}E-^{A}E. The novel reactivity of $^{A}E_2{}^{B}E_2$ σ(4c–6e) in **I** was also clarified [8].

σ(4c–6e) is the first member of σ(*m*c–*n*e: $4 \le m$; $m < n < 2m$) [7–13]. The σ(4c–6e) interactions are strongly suggested to play an important role in the development of high functionalities in materials and in the key processes of biological and pharmaceutical activities, recently. The bonding is applied to a wide variety of fields, such as crystal engineering, supramolecular soft matters, and nanosciences [4, 14–23]. The nature of ^{B}E---^{A}E and ^{A}E-^{A}E in ^{B}E---^{A}E-^{A}E---^{B}E of $^{A}E_2{}^{B}E_2$ σ(4c–6e) has been elucidated [24–27] using the quantum theory of atoms in molecules (QTAIM) approach, introduced by Bader [28–37]. The linear interactions of the σ(4c–6e) type will form if ^{B}E in $^{A}E_2{}^{B}E_2$ is replaced by *X*, giving E_2X_2 σ(4c–6e). The nature of E_2X_2 σ(4c–6e) in the naphthalene system of 1-(8-X$C_{10}H_6$)E-

E($C_{10}H_6X$-8′)-1′ [**II** (E, *X*) = (S, Cl), (S, Br), (Se, Cl), and (Se, Br)] was similarly clarified very recently [38].

The σ(4c–6e) interaction will also be produced even if both ^{B}E and ^{A}E in $^{A}E_2{}^{B}E_2$ are replaced by *X*. X_4 σ(4c–6e) should also be stabilized through CT of the $n_p(X) \longrightarrow \sigma*$(X-X) $\leftarrow n_p(X)$ form. The energy lowering of the system through the CT interaction must be the driving force for the formation of X_4 σ(4c–6e). X_4 σ(4c–6e) is the typical kind of halogen bonds, together with E_2X_2 σ(4c–6e), which are of current and continuous interest [39]. Br_4 σ(4c–6e) has been clearly established in the selenanthrene system, $SeC_{12}H_8$(Br) Se**Br**---**Br**-**Br**---**Br**Se(Br)$C_{12}H_8$Se (**1**), through the preparation and the structural determination by the X-ray crystallographic analysis [39]. The atoms taking part in the linear interaction in question are shown in bold. The structure of ($BrSeC_{12}H_8$)**Br**---**Se**---**Br**-**Br**---**Br**-**Se**($C_{12}H_8$Se)-**Br** (**2**) was also reported, in addition to **1**, which is suggested to contain Se_2Br_5 σ(7c–10e) since the seven atoms of Se_2Br_5 align almost linearly in crystals. Figure 1 shows the structures of **1** and **2** determined by the X-ray analysis and the approximate MO model for σ(4c–6e) and σ(7c–10e).

It is challenging to elucidate the nature of Br_4 σ(4c–6e) of the n_p(Br) $\longrightarrow \sigma*$(Br-Br)$\leftarrow n_p$(Br) form in **1** and Se_2Br_5 σ(7c–10e) in **2**, together with the related species. Figure 2 illustrates the process assumed for the formation of **1** and **2** from selenanthrene (**S**: $SeC_{12}H_8Se$). In this process, ($SeC_{12}H_8$)**Br**-**Se**-**Br** (**3**) should be formed first in the reaction of **S** with $\mathbf{Br}_2$, and then **3** reacts with $\mathbf{Br}_2$ to yield **Br**[Se(Br)($C_{12}H_8$)]**Se**---**Br**-**Br** (**4**). The almost linear alignment of **Br**---**Se**---**Br**-**Br** in **4** could be analysed by the $SeBr_3$ σ(4c–6e) model, where the **Br** and **Se** atoms in **4** are placed in close proximity in space. While **1** containing Br_4 σ(4c–6e) forms in the reaction of (**3** + Br_2 + **3**), the reaction of **3** + **4** yields **2**, consisting Se_2Br_5 σ(7c–10e). Both **1** and **2** are recognized as the Br_2-included species. While XC_4H_4(Br) Se**Br**---**Br**-**Br**---**Br**Se(Br)C_4H_4X (**5** (*X* = Se) and **6** (*X* = S)), models of **1**, also consisted of Br_4 σ(4c–6e), Se_2Br_5 σ(7c–10e) will appear typically in the anionic species, [**Br**-**Se**(Me_2)-**Br**---**Br**---**Br**-**Se**(Me_2)-**Br**]$^-$ (**7**) and [**Br**-**Se**(SeC_4H_4)-**Br**---**Br**---**Br**-**Se**(C_4H_4Se)-**Br**]$^-$ (**8**), models of **2**. Species, **5**, **6**, **7**, and **8**, are shown in Figure 2, where **5**, **6**, and **8** belong to the 1,4-diselenin system.

What are the differences and similarities between X_4 σ(4c–6e), E_4 σ(4c–6e), and E_2X_2 σ(4c–6e)? The nature of X_4 σ(4c–6e) in **1** (*X* = Br) is to be elucidated together with the models. Models, other than **5** and **6**, are also devised to examine the stabilization sequence of Br_4 σ(4c–6e). H_2Br_4 (C_{2h}) and Me_2Br_4 (C_{2h}) have the form of R-**Br**---**Br**-**Br**---**Br**-R (RBr_4R: R = H and Me), which are called the model group **A** (G(**A**)). The electronic efficiency to stabilize Br_4 σ(4c–6e) seems small for R in G(**A**). Br_6 (C_{2h}) is detected as the partial structure in the crystals of Br_2 [40]. Br_6 (C_{2h}) in the crystals is denoted by Br_6 $(C_{2h})_{obsd}$. The optimized structure of Br_6 (C_{2h}) has one imaginary frequency, which belongs to G(**A**), together with Br_6 $(C_{2h})_{obsd}$. The optimized structure of Br_6 retains the C_2 symmetry, (Br_6 (C_2)), which also belongs to G(**A**). The CT interaction of the $n_p(^{B}Br) \longrightarrow \sigma*(^{A}Br\text{-}^{A}Br) \longleftarrow n_p(^{B}Br)$ form in Br_4 σ(4c–6e) will be much stabilized if the large negative charge is developed at the ^{B}Br atoms in Br-(R_2)Se-^{B}**Br**---^{A}**Br**-^{A}**Br**---^{B}**Br**-Se(R_2)-Br, where the $\angle Se^{B}\mathbf{Br}^{A}\mathbf{Br}$ is around 90°. The highly negatively charged ^{B}**Br** in Br-Se(R_2)-^{B}**Br** (R = H and Me) of σ(3c–4e) is employed to stabilize Br_4 σ(4c–6e), in this case. The models form G(**B**). The nature of Br_4 σ(4c–6e) in **5** and **6** is similarly analysed, which belongs to G(**B**). Br_4^{2-} ($D_{\infty h}$) also belongs to G(**B**) although one imaginary frequency was predicted for Br_4^{2-}, if optimized at the MP2 level. Figure 3 illustrates the story for the stabilization of Br_4 σ(4c–6e) in the sequence of the species, starting from G(**A**) to **1**, *via* G(**B**). Figure 3 also shows the ^{A}Br-^{A}Br and ^{A}Br---^{B}Br distances ($r(^{A}Br\text{-}^{A}Br)$ and $r(^{A}Br\text{-}^{B}Br)$, respectively), together with the charge developed at ^{B}Br in the original species of R-^{B}Br (*Qn* (^{B}Br)), which construct R-^{B}Br---^{A}Br-^{A}Br---^{B}Br-R.

A chemical bond or interaction between atoms A and B is denoted by A-B, which corresponds to a bond path (BP) in the quantum theory of atoms in molecules (QTAIM) approach, introduced by Bader [28–37]. We will use A-∗-B for BP, where the asterisk emphasizes the existence of a bond critical point (BCP, ∗) in A-B [28, 29]. (Dots are usually employed to show BCPs in molecular graphs. Therefore, A-•-B would be more suitable to describe the BP with a BCP. Nevertheless, A-∗-B is employed to emphasize the existence of a BCP on the BP in question in our case. BCP is a point along BP at the interatomic surface, where $\rho(\mathbf{r})$ (charge density) reaches a minimum along the interatomic (bond) path, while it is a maximum on the interatomic surface separating the atomic basins). The chemical bonds and interactions are usually classified by the signs of Laplacian rho ($\nabla^2\rho_b(\mathbf{r}_c)$) and $H_b(\mathbf{r}_c)$ at BCPs, where $\rho_b(\mathbf{r}_c)$ and $H_b(\mathbf{r}_c)$ are the charge densities and total electron energy densities at BCPs, respectively (see Scheme S1 in Supplementary File). The relations between $H_b(\mathbf{r}_c)$, $\nabla^2\rho_b(\mathbf{r}_c)$, $G_b(\mathbf{r}_c)$ (the kinetic energy densities), and $V_b(\mathbf{r}_c)$ (the potential energy densities) are represented in equations (1) and (2):

$$H_b(\mathbf{r}_c) = G_b(\mathbf{r}_c) + V_b(\mathbf{r}_c), \tag{1}$$

$$\left(\frac{\hbar^2}{8m}\right)\nabla^2\rho_b(\mathbf{r}_c) = H_b(\mathbf{r}_c) - \frac{V_b(\mathbf{r}_c)}{2} = G_b(\mathbf{r}_c) + \frac{V_b(\mathbf{r}_c)}{2}. \tag{2}$$

How can the nature of Br_4 σ(4c–6e) and Se_2Br_5 σ(7c–10e) be clarified? For the characterization of interactions in more detail, we recently proposed QTAIM dual functional analysis (QTAIM-DFA) [42–47] for experimental chemists to analyze their own chemical bonds and interaction results based on their own expectations, according to the QTAIM approach [28–37]. $H_b(\mathbf{r}_c)$ is plotted versus $H_b(\mathbf{r}_c) - V_b(\mathbf{r}_c)/2$ (= $(\hbar^2/8m)\nabla^2\rho_b(\mathbf{r}_c)$) at BCPs in QTAIM-DFA. The classification of interactions by the signs of $\nabla^2\rho_b(\mathbf{r}_c)$ and $H_b(\mathbf{r}_c)$ is incorporated in QTAIM-DFA. Data from the fully optimized structures correspond to the static natures of the interactions, which are analysed using the polar coordinate (R, θ), representation [42, 44–46]. Each interaction plot, containing data from both the perturbed structures and the fully optimized one include a specific curve that provides important information about the interaction. This plot is expressed by (θ_p, κ_p), where θ_p

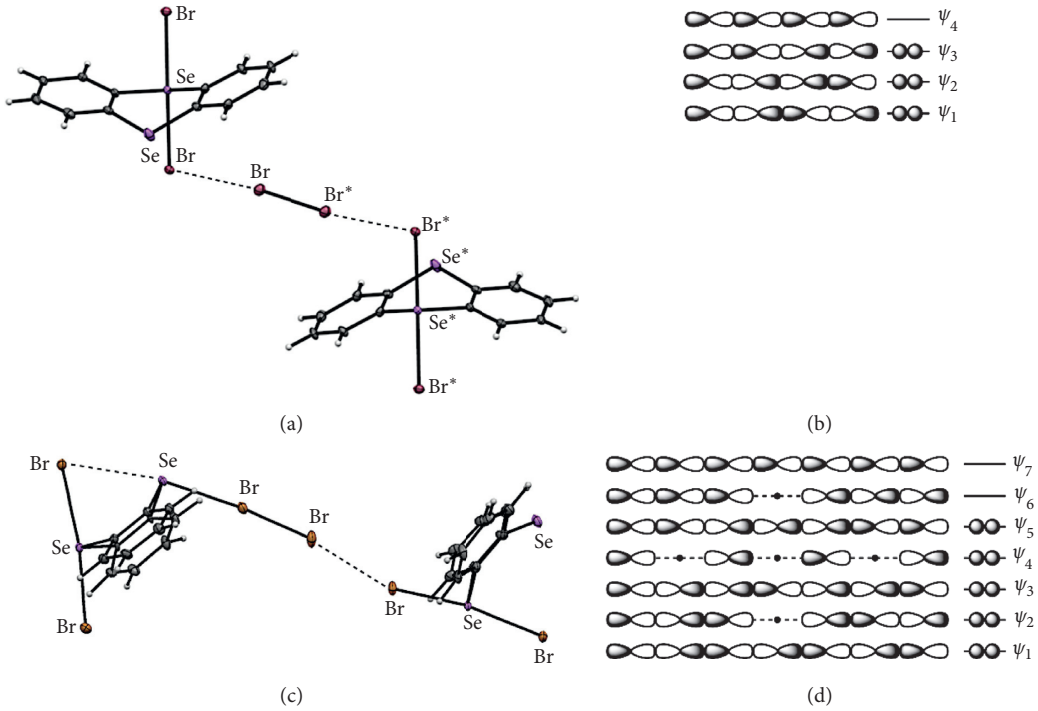

Figure 1: Structure of **1** determined by the X-ray crystallographic analysis (a) and the approximate MO model for σ(4c–6e) (b); structure of **2** (c) and the approximate MO model for σ(7c–10e) (d).

corresponds to the tangent line of the plot and κ_p is the curvature. The concept of the dynamic nature of interactions has been proposed based on (θ_p, κ_p) [42, 44]. θ and θ_p are measured from the y-axis and the y-direction, respectively. We call (R, θ) and (θ_p, κ_p) QTAIM-DFA parameters, which are drawn in Figure 4, exemplified by Br_4^{2-} ($D_{\infty h}$). While (R, θ) classifies the interactions, (θ_p, κ_p) characterizes them.

We proposed a highly reliable method to generate the perturbed structures for QTAIM-DFA very recently [48]. The method is called CIV, which employs the coordinates derived from the compliance force constants C_{ij} for the internal vibrations. Compliance force constants C_{ij} are defined as the partial second derivatives of the potential energy due to an external force, as shown in equation (3), where i and j refer to the internal coordinates and the force constants f_i and f_j correspond to i and j, respectively. The C_{ij} values and the coordinates corresponding to the values can be calculated using the compliance 3.0.2 program, released by Brandhorst and Grunenberg [49–52]. The dynamic nature of interactions based on the perturbed structures with CIV is described as the "intrinsic dynamic nature of interactions" since the coordinates are invariant to the choice of the coordinate system:

$$C_{ij} = \frac{\partial^2 E}{\partial f_i \partial f_j}. \quad (3)$$

QTAIM-DFA has excellent potential for evaluating, classifying, characterizing, and understanding weak to strong interactions according to a unified form. The superiority of QTAIM-DFA to elucidate the nature of interactions, employing the perturbed structures generated with CIV, is explained in the previous papers [48, 53] (see also Figure S2 and Table S2 in Supplementary File). QTAIM-DFA is applied to standard interactions and rough criteria that distinguish the interaction in question from others which are obtained. QTAIM-DFA and the criteria are explained in Supplementary File using Schemes S1–S3, Figures S1 and S2, Table S1, and equations (S1)–(S7). The basic concept of the QTAIM approach is also explained.

We consider QTAIM-DFA, employing the perturbed structures generated with CIV, to be well suited to elucidate the nature of Br_4 σ(4c–6e) in **1**, Se_2Br_5 σ(7c–10e) in **2**, and the models derived from **1** and **2**, together with the related linear interactions. The interactions in Br_4 σ(4c–6e) are denoted by ^{B}Br-$*$-^{A}Br-$*$-^{A}Br-$*$-^{B}Br, where the asterisk emphasizes the existence of a BCP in the interactions, so are those in Se_2Br_5 σ(7c–10e). Herein, we present the results of the investigations on the extended hypervalent interactions in the species, together with the structural feature. Each interaction is classified and characterized, employing the criteria as a reference.

2. Methodological Details in Calculations

Calculations were performed employing the Gaussian 09 programs package [54]. The basis sets employed for the calculations were obtained, as implemented from Sapporo Basis Set Factory [55]. The basis sets of the (621/31/2), (6321/621/3), (74321/7421/72), and (743211/74111/721/2+1s1p) forms were employed for C, S, Se, and Br, respectively, with the (31/3) form for H. The basis set system is called BSS-A.

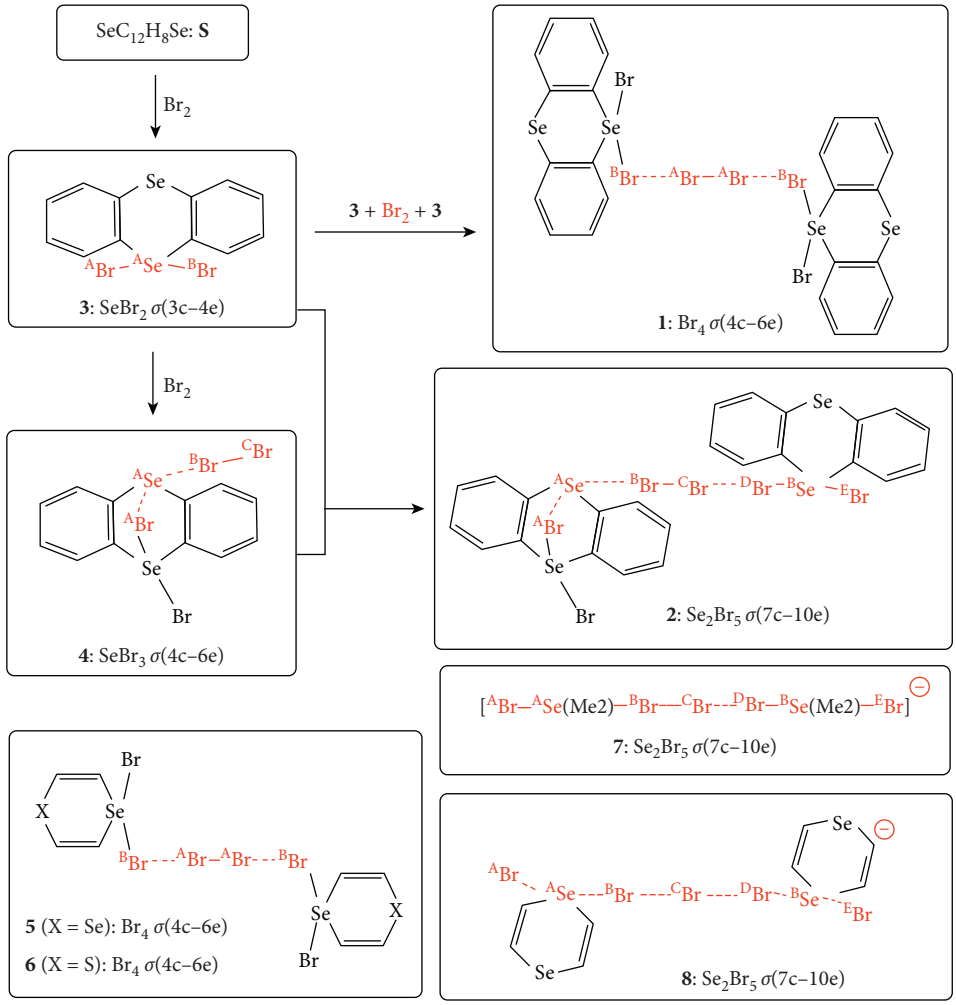

FIGURE 2: Process assumed for the formation of Br_4 σ(4c–6e) in **1** from $Se(C_{12}H_8)Se$ (**S**) *via* **3** and Se_2Br_5 σ(7c–10e) in **2** *via* **3** and **4**. **5** and **6** with Br_4 σ(4c–6e), models of **1**, and **7** and **8** with Se_2Br_5 σ(7c–10e), models of **2**, are also shown. Atoms taking part in the linear interactions are shown by red.

All species were calculated employing BSS-A, and the Møller–Plesset second-order energy correlation (MP2) level [56–58] was applied for the optimizations. Optimized structures were confirmed by the frequency analysis. The results of the frequency analysis were used to calculate the C_{ij} values and the coordinates ($\mathbf{C}_i$) corresponding to the values. The DFT level of CAM-B3LYP [59] was also applied when necessary. The QTAIM functions were analysed with the AIM2000 [60] and AIMAll [61] programs.

The method to generate perturbed structures with CIV is the same as that explained in the previous papers [48, 53]. As shown in equation (4), the i-th perturbed structure in question ($\mathbf{S}_{iw}$) is generated by the addition of the i-th coordinates ($\mathbf{C}_i$), derived from C_{ij}, to the standard orientation of a fully optimized structure ($\mathbf{S}_o$) in the matrix representation. The coefficient f_{iw} in equation (4) controls the structural difference between $\mathbf{S}_{iw}$ and $\mathbf{S}_o$: f_{iw} is determined to satisfy equation (5) for r, where r and r_o stand for the interaction distances in question in the perturbed and fully optimized structures, respectively, with $a_o = 0.52918$ Å (Bohr radius). The $\mathbf{C}_i$ values of five digits are used to predict $\mathbf{S}_{iw}$:

$$\mathbf{S}_{iw} = \mathbf{S}_o + f_{iw} \cdot C_i, \tag{4}$$

$$r = r_o + wa_o, \quad \left(w = (0), \pm 0.05, \text{and } \pm 0.1;\ a_o = 0.52918\ \text{Å}\right), \tag{5}$$

$$y = c_o + c_1 x + c_2 x^2 + c_3 x^3, \quad \left(R_c^2\text{: square of correlation coefficient}\right). \tag{6}$$

In QTAIM-DFA, $H_b(\mathbf{r}_c)$ is plotted versus $H_b(\mathbf{r}_c) - V_b(\mathbf{r}_c)/2$ for data of $w = 0$, ±0.05, and ±0.10 in equation (5). Each plot is analysed using a regression curve of the cubic function, as shown in equation (6), where $(x, y) = (H_b(\mathbf{r}_c) - V_b(\mathbf{r}_c)/2$ and $H_b(\mathbf{r}_c))$ (R_c^2 (square of correlation coefficient) > 0.99999 in usual) [46].

3. Results and Discussion

3.1. Structural Optimizations. The structures of **1** (C_i) and **2** (C_1) determined by the X-ray analysis are denoted by **1**

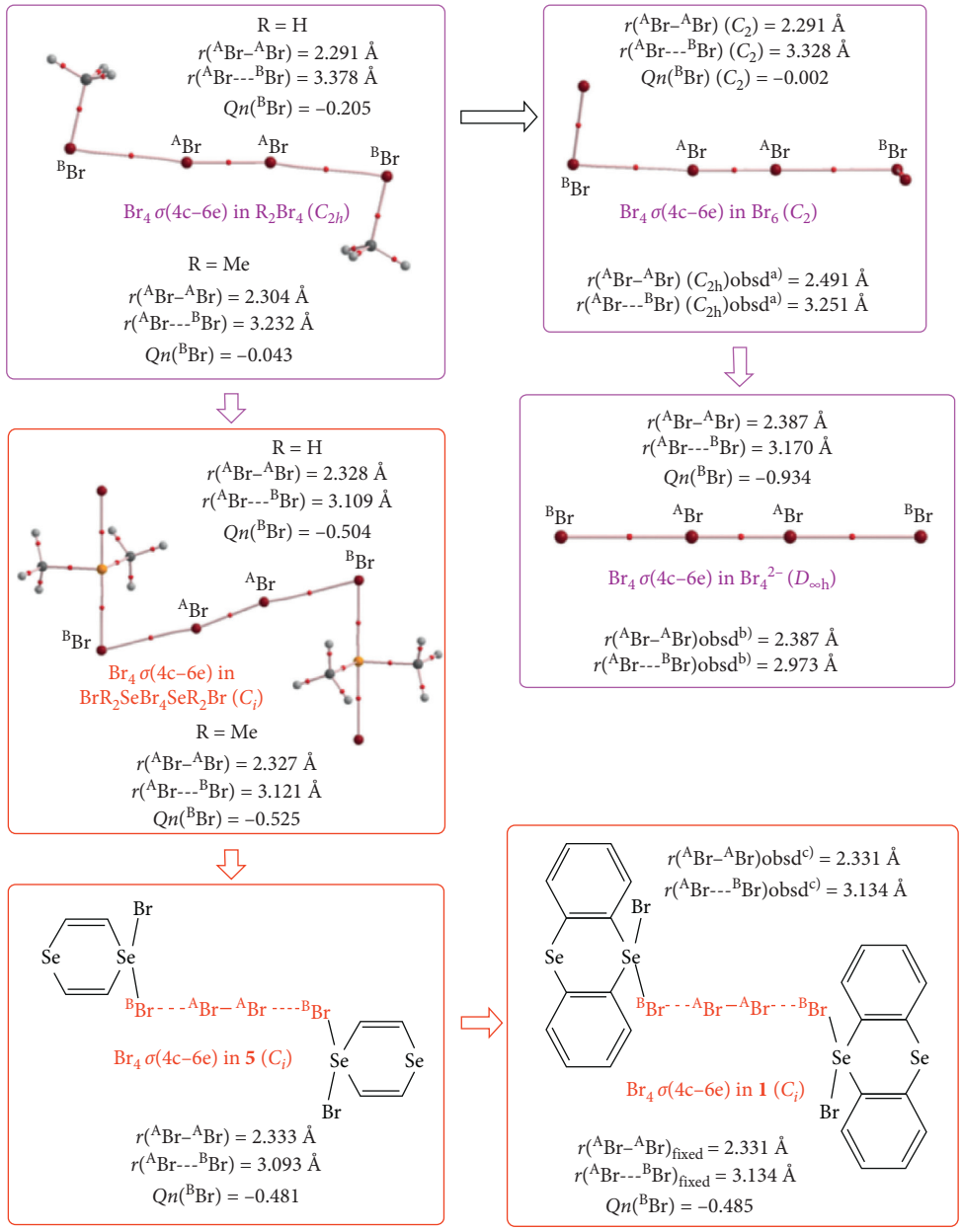

(a) Ref. [40] (b) Ref. [41] (c) Ref. [39]

FIGURE 3: Sequence in the stabilization of Br_4 σ(4c–6e), starting from those in G(**A**) to **1** via those of G(**B**).

$(C_i)_{obsd}$ and **2** $(C_1)_{obsd}$, respectively [39]. The structural parameters are shown in Tables S2 and S3 in Supplementary File, respectively. Figure 3 contains the selected structural parameters for **1** $(C_i)_{obsd}$. The structures are optimized for G(**A**) of H_2Br_4 (C_{2h}), Me_2Br_4 (C_{2h}), Br_6 (C_{2h}), and Br_6 (C_2) and G(**B**) of $H_4Se_2Br_6$ (C_i), $Me_4Se_2Br_6$ (C_i), **5** (C_i), and **6** (C_i), together with **3** (C_s), **4** (C_s), **7** (C_{2h}), **8** (C_{2h}), and Br_2 ($D_{\infty h}$). The optimized structural parameters are also collected in Tables S2 and S3 in Supplementary File. The frequency analysis was successful for the optimized structures, except for **1** $(C_i)_{obsd}$ and Br_6 (C_{2h}). All positive frequencies were obtained for **1** (C_i), if calculated with CAM-B3LYP/BSS-A, which confirms the structure. The Br---Br distances of Br_4 σ(4c–6e) in **1** (C_i) are somewhat longer if optimized at the CAM-B3LYP level, relative to **1** $(C_i)_{obsd}$. While one imaginary frequency is detected in Br_6 (C_{2h}), Br_6 (C_2) has all positive frequencies. The optimized structures are not shown in figures, instead, some of them can be found in Figures 3 and 5, where the molecular graphs are drawn on the optimized structures. Figure 3 contains the optimized $r(^{A}Br\text{-}^{A}Br)$ and $r(^{A}Br\text{-}^{B}Br)$ distances for the models and the charge developed at ^{B}Br in the original R-^{B}Br and Br-(R_2)Se-^{B}Br (Qn (^{B}Br)), which give the models of G(**A**) and G(**B**), respectively. The $r(^{A}Br\text{-}^{B}Br)$ values become shorter in the order shown in equation (7), if evaluated with MP2/BSS-A:

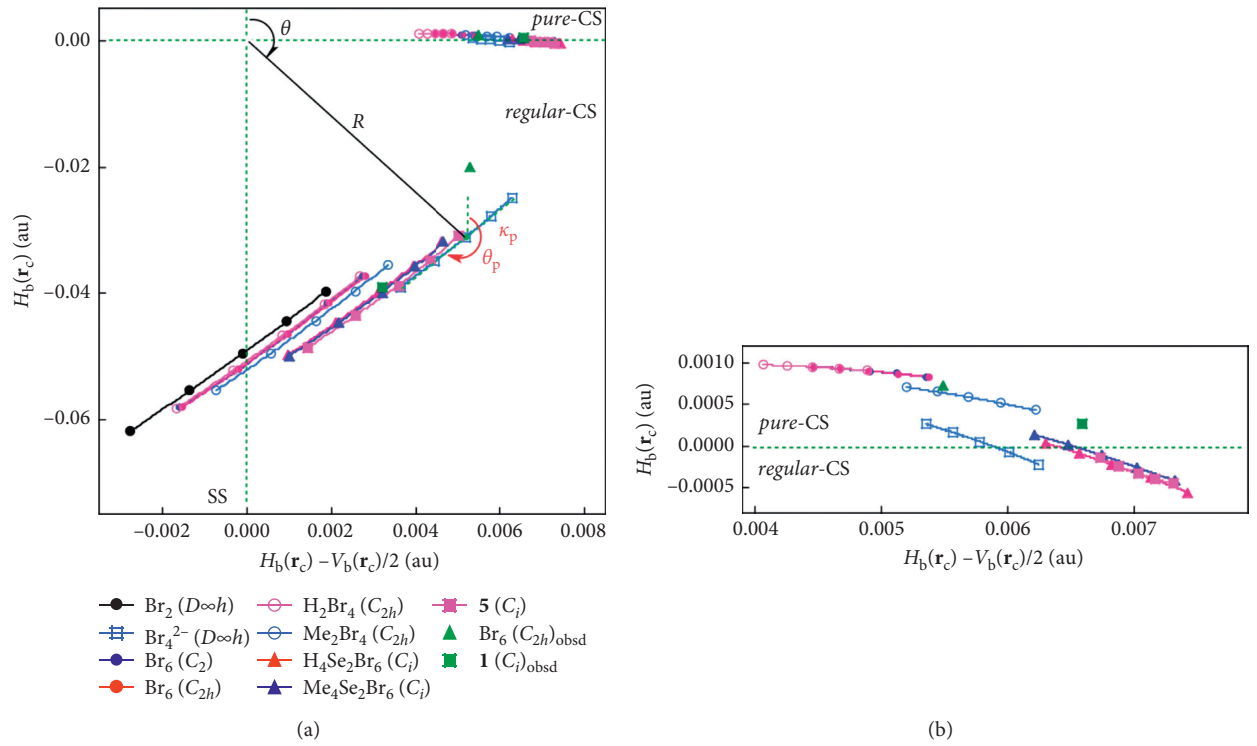

FIGURE 4: QTAIM-DFA plots of $H_b(\mathbf{r}_c)$ versus $H_b(\mathbf{r}_c) - V_b(\mathbf{r}_c)/2$ for ^{A}Br-∗-^{A}Br (a) and ^{A}Br-∗-^{B}Br (b) in Br_4 σ(4c–6e) of the species in Table 1, together with those of the perturbed structures generated with CIV. Marks and colours for the species are shown in the figure.

$r(^{A}\mathrm{Br} - {}^{B}\mathrm{Br})$:

$$\mathrm{H_2Br_4}\,(C_{2h}) > \mathbf{1}\,(C_i)\mathrm{CAM} > \mathrm{Br_6}\,(C_2 \text{ and } C_{2h}) > \mathrm{Br_6}\,(C_{2h})_{\mathrm{obsd}}[40] > \mathrm{Me_2Br_4}\,(C_{2h}) > \mathrm{Br_4^{2-}}\,(D_{\infty h}) > \mathbf{1}\,(C_i)_{\mathrm{obsd}} \geq \mathrm{Me_4Se_2Br_6}\,(C_i) \geq \mathrm{H_4Se_2Br_6}\,(C_i) > \mathbf{5}\,(C_i) \geq \mathbf{6}\,(C_i). \quad (7)$$

One imaginary frequency was also predicted for Br_4^{2-} ($D_{\infty h}$) if optimized with MP2/BSS-A. Br_4^{2-} ($D_{\infty h}$) seems to collapse to Br_3^- and Br^-, according to the imaginary frequency. The double negative charges in Br_4^{2-} ($D_{\infty h}$) would be responsible for the results. The electrostatic repulsion between the double negative charges will operate to collapse it.

3.2. Energies for Formation of Br_4 σ(4c–6e) and NBO Analysis. Energies for the formation of R′**Br_4**R′ from the components (2R′**Br** + **Br_2**) (ΔE) are defined by equation (8). The ΔE values evaluated on the energy surface are denoted by ΔE_{ES}, while those corrected with the zero-point energies are by ΔE_{ZP}. The ΔE_{ES} and ΔE_{ZP} values for the optimized structures are given in Table S2 in Supplementary File. ΔE_{ZP} are excellently correlated to ΔE_{ES} ($\Delta E_{ZP} = 0.99\Delta E_{ES} + 1.93$: $R_c^2 = 0.9998$, see Figure S3 in Supplementary File):

$$\Delta E\left(R_2'\mathrm{Br}_4\right) = E\left(R_2'\mathrm{Br}_4\right) - \left[2E\left(R'\mathrm{Br}\right) + E\left(\mathrm{Br}_2\right)\right], \quad (8)$$

$$E(2) = q_i \times \frac{F(i,j)^2}{\left(\varepsilon_j - \varepsilon_i\right)}. \quad (9)$$

NBO analysis [62] was applied to ^{A}Br---^{B}Br of the species to evaluate the contributions from CT to stabilize R′-^{B}Br---^{A}Br-^{A}Br---^{B}Br-R′. For each donor NBO (i) and acceptor NBO (j), the stabilization energy $E(2)$ is calculated based on the second-order perturbation theory in NBO, according to equation (9), where q_i is the donor orbital occupancy, ε_i and ε_j are diagonal elements (orbital energies), and $F(i, j)$ is the off-diagonal NBO Fock matrix element. The results are collected in Table S4 in Supplementary File. The ΔE_{ES} values are very well correlated to $E(2)$ for the optimized structures, except for Br_4^{2-} ($D_{\infty h}$). ($\Delta E_{ES} = -0.71(2E(2)) + 7.17$: $R_c^2 = 0.959$, see Figure S4 in Supplementary File). Br_4^{2-} ($D_{\infty h}$) is predicted to be less stable than the components.

Before application of QTAIM-DFA to Br_4 σ(4c–6e) and Se_2Br_5 σ(7c–10e), molecular graphs were examined, as shown in the next section.

3.3. Molecular Graphs with Contour Plots for the Species Containing Br_4 σ(4c–6e), Se_2Br_5 σ(7c–10e), and Related Linear Interactions. Figure 5 illustrates the molecular graphs of **5** (C_i), **6** (C_i), **7** (C_{2h}), and **8** (C_{2h}), drawn on the optimized structures, together with **1** $(C_i)_{obsd}$ and **2** $(C_1)_{obsd}$. Figure 5 also shows the contour plots of $\rho(r)$ drawn on the suitable plane in the molecular graphs. BCPs are well demonstrated to locate on the (three-dimensional) saddle points of $\rho(r)$. Molecular graphs of Me_2Br_4 (C_{2h}), Br_6 (C_2), Br_4^{2-} ($D_{\infty h}$), and $Br(Me_2)SeBr_4Se(Me_2)Br$ (C_i) are shown in Figure 3, which are drawn on the optimized structures.

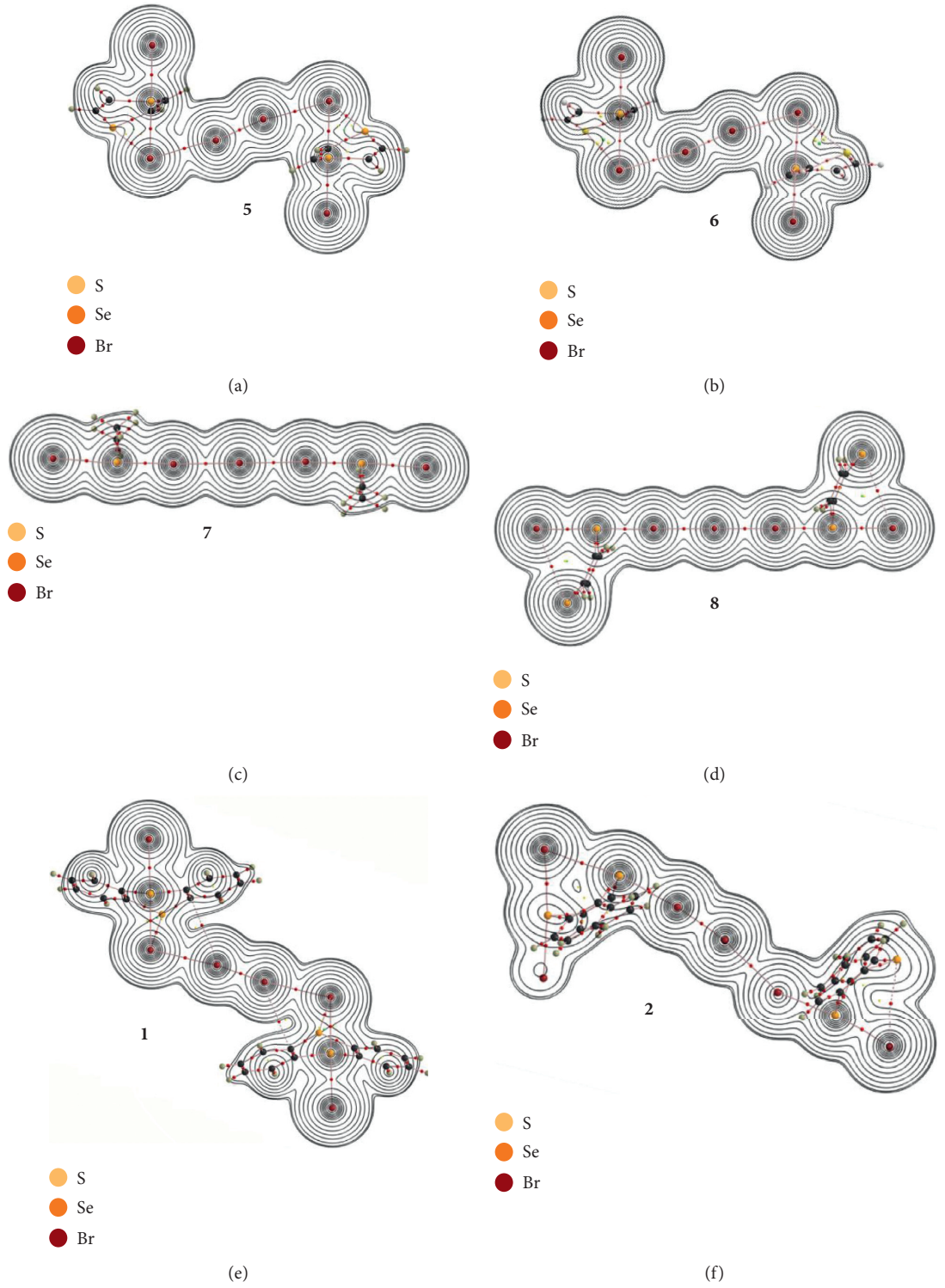

FIGURE 5: Molecular graphs of **5** (C_i) (a), **6** (C_i) (b), **7** (C_{2h}) (c), and **8** (C_{2h}) (d) drawn on the structures optimized at the MP2 level, together with **1** $(C_i)_{obsd}$ (e) and **2** $(C_1)_{obsd}$ (f). Contour plots of $\rho(\mathbf{r})$ are also drawn on the planes containing the linear interactions. BCPs are denoted by red dots, RCPs (ring critical points) by yellow dots, and CCPs (cage critical points) by green dots. BPs (bond paths) are drawn as pink lines and the secondary ones as pink dots. They are associated with the BCPs. Carbon and hydrogen atoms are shown in black and gray, respectively. The contours (ea_o^{-3}) are at 2^l ($l = \pm 8, \pm 7, \ldots$, and 0).

3.4. Survey of Br_4 σ(4c–6e) and Se_2Br_5 σ(7c–10e). BPs in Br_4 σ(4c–6e) and Se_2Br_6 σ(7c–10e) seem straight, as shown in Figures 3 and 5. To show the linearity more clearly, the lengths of BPs (r_{BP}) for Br_4 σ(4c–6e) are calculated. The values are collected in Table S5 in Supplementary File, together with the corresponding straight-line distances (R_{SL}).

The table contains the values for Se_2Br_6 σ(7c–10e) in **7** (C_{2h}) and **8** (C_{2h}). The differences between them ($\Delta r_{BP} = r_{BP} - R_{SL}$) are less than 0.003 Å. The r_{BP} values are plotted versus R_{SL}, which are shown in Figure S5 in Supplementary File. The correlations are excellent, as shown in the figure. Therefore, Br_4 σ(4c–6e) and Se_2Br_6 σ(7c–10e) in the species can be approximated by the straight lines.

QTAIM functions are calculated for Br_4 σ(4c–6e) at BCPs. Table 1 collects the values for the interactions. $H_b(\mathbf{r}_c)$ is plotted versus $H_b(\mathbf{r}_c) - V_b(\mathbf{r}_c)/2$ for the data shown in Table 1, together with those from the perturbed structures generated with CIV. Figure 4 shows the plots for the ^{A}Br-∗-^{A}Br and ^{A}Br-∗-^{B}Br interactions in Br_4 σ(4c–6e) of the bromine species. The plots for ^{A}Br-∗-^{A}Br appear in the region of $H_b(\mathbf{r}_c) - V_b(\mathbf{r}_c)/2 > 0$ and $H_b(\mathbf{r}_c) < 0$, for all species, except for the original Br_2 ($D_{\infty h}$), of which the plot appears in the region of $H_b(\mathbf{r}_c) - V_b(\mathbf{r}_c)/2 < 0$ and $H_b(\mathbf{r}_c) < 0$. Therefore, the interactions are all classified by the *regular*-CS (closed shell) interactions, except for Br_2 ($D_{\infty h}$), which is classified by the SS (shard shell) interaction. On the contrary, data of ^{A}Br-∗-^{B}Br appear in the region of $H_b(\mathbf{r}_c) - V_b(\mathbf{r}_c)/2 > 0$ and $H_b(\mathbf{r}_c) > 0$ for all species, except for those in $H_4Se_2Br_6$ (C_i), $Me_4Se_2Br_6$ (C_i), **5** (C_i), and **6** (C_i), which appear in the region of $H_b(\mathbf{r}_c) - V_b(\mathbf{r}_c)/2 > 0$ and $H_b(\mathbf{r}_c) < 0$. As a result, ^{A}Br-∗-^{B}Br is classified by the *pure*-CS interactions (*p*-CS) for all, except for the four species, of which ^{A}Br-∗-^{B}Br is classified by the *regular*-CS interactions (*r*-CS). The ^{A}Br-∗-^{B}Br interaction in Br_4^{2-} ($D_{\infty h}$) is very close to the borderline between *p*-CS and *r*-CS since $H_b(\mathbf{r}_c) = 0.0001$ au for Br_4^{2-} ($D_{\infty h}$), which is very close to zero. QTAIM-DFA parameters of (R, θ) and (θ_p, κ_p) are obtained by analysing the plots of $H_b(\mathbf{r}_c)$ versus $H_b(\mathbf{r}_c) - V_b(\mathbf{r}_c)/2$ in Figure 4, according to equations (S3)–(S6). Table 1 collects the QTAIM-DFA parameters for Br_4 σ(4c–6e). The classification of interactions will also be discussed based on the (R, θ) values.

QTAIM functions are similarly calculated for Se_2Br_6 σ(7c–10e) at BCPs, together with the related interactions. $H_b(\mathbf{r}_c)$ is similarly plotted versus $H_b(\mathbf{r}_c) - V_b(\mathbf{r}_c)/2$ although not shown in the figures. Then, QTAIM-DFA parameters of (R, θ) and (θ_p, κ_p) are obtained by analysing the plots, according to equations (S3)–(S6). Table 2 collects the QTAIM-DFA parameters of (R, θ) and (θ_p, κ_p) for Br_4 σ(4c–6e).

3.5. Nature of Br_4 σ(4c–6e). Interactions are characterized by (R, θ), which correspond to the data from the fully optimized structures. On the contrary, they are characterized employing (θ_p, κ_p) derived from the data of the perturbed structures around the fully optimized structures and the fully optimized ones. In this case, the nature of interactions is substantially determined based of the (R, θ, θ_p) values, while the κ_p values are used only additionally. It is instructive to survey the criteria before detail discussion. The criteria tell us that $180^\circ < \theta$ ($H_b(\mathbf{r}_c) - V_b(\mathbf{r}_c)/2 < 0$) for the SS interactions, $90^\circ < \theta < 180^\circ$ ($H_b(\mathbf{r}_c) < 0$) for the *r*-CS interactions, and $45^\circ < \theta < 90^\circ$ ($H_b(\mathbf{r}_c) > 0$) for *p*-CS interactions. The θ_p value characterizes the interactions. In the *p*-CS region of $45^\circ < \theta < 90^\circ$, the character of interactions will be the vdW type for $45^\circ < \theta_p < 90^\circ$, whereas it will be the typical HB type without covalency (*t*-HB_{nc}) for $90^\circ < \theta_p < 125^\circ$, where $\theta_p = 125^\circ$ is tentatively given for $\theta = 90^\circ$. The CT interaction will appear in the *r*-CS region of $90^\circ < \theta < 180^\circ$. The *t*-HB type with covalency (*t*-HB_{wc}) appears in the region of $125^\circ < \theta_p < 150^\circ$ ($90^\circ < \theta < 115^\circ$), where ($\theta$, θ_p) = (115°, 150°) is tentatively given as the borderline between *t*-HB_{wc} and the CT-MC nature. The borderline for the interactions between CT-MC and CT-TBP types is defined by $\theta_p = 180^\circ$. $\theta = 150^\circ$ is tentatively given for $\theta_p = 180^\circ$. Classical chemical bonds of SS ($180^\circ < \theta$) will be strong (Cov-s) when $R > 0.15$ au, whereas they will be weak (Cov-w) for $R < 0.15$ au. The classification and characterization of interactions are summarized in Table S1 and Scheme S3 in Supplementary File.

The ^{A}Br-∗-^{A}Br and ^{A}Br-∗-^{B}Br interactions of Br_4 σ(4c–6e) will be classified and characterized based on the (R, θ, θ_p) values, employing the standard values as a reference (see Scheme S2 in Supplementary File). $R < 0.15$ au for all interactions in Table 1; therefore, no Cov-s were detected in this work. The (θ, θ_p) values are (180.1°, 191.8°) for the original Br_2 ($D_{\infty h}$) if evaluated with MP2/BSS-A. Therefore, the nature of Br-∗-Br in Br_2 ($D_{\infty h}$) is classified by the SS interactions and characterized as the Cov-w nature, which is denoted by SS/Cov-w. The (θ, θ_p) values are (170.6–179.0°, 190.6–191.7°) for ^{A}Br-∗-^{A}Br of Br_4 σ(4c–6e) in the optimized structures in Table 1, of which nature is *r*-CS/CT-TBP. The (θ, θ_p) values are (78.0–84.1°, 94.7–105.1°) for ^{A}Br-∗-^{B}Br in the optimized structures of Br_6 (C_2), Br_6 (C_{2h}), and R_2Br_4 (C_{2h}) (R = H and Me); therefore, the nature is predicted to be *r*-CS/*t*-HB_{wc}. The nature of ^{A}Br-∗-^{B}Br in $R_4Se_2Br_6$ (C_i) (R = H and Me), **5** (C_i) and **6** (C_i), is *r*-CS/*t*-HB_{wc}, judging from the (θ, θ_p) values of (90.9–92.8°, 116.4–122.5°). The calculated (θ, θ_p) values of ^{A}Br-∗-^{A}Br and ^{A}Br-∗-^{B}Br for the optimized structure of Br_4^{2-} ($D_{\infty h}$) are (170.6°, 190.6°) and (89.5°, 118.2°), respectively. In this case, ^{A}Br-∗-^{A}Br and ^{A}Br-∗-^{B}Br are predicted to have the nature of *r*-CS/CT-TBP and *p*-CS/*t*-HB_{nc}, respectively. However, ^{A}Br-∗-^{B}Br is just the borderline region to the *r*-CS interactions with $\theta = 89.5^\circ$. The characteristic nature of the ^{B}E---^{A}E-^{A}E---^{B}E interactions in Br_4^{2-} ($D_{\infty h}$) would be controlled by the double negative charges in the species.

The results in Table 1 show that the ^{A}Br-∗-^{A}Br interaction in Br_4 σ(4c–6e) becomes weaker, as the strength of the corresponding ^{A}Br-∗-^{B}Br increases. The strength of ^{A}Br-∗-^{A}Br becomes weaker in the order shown in equation (10), if evaluated by θ, while that of ^{A}Br-∗-^{B}Br increases in the order shown in equation (11), if measured by θ. Very similar results were obtained by θ_p:

$$\begin{aligned} &\theta \text{ for } {}^{A}\text{Br} - * - {}^{A}\text{Br}: \\ &\text{Br}_2\,(D_{\infty h}) > \text{H}_2\text{Br}_4\,(C_{2h}) \geq \text{Br}_6\,(C_2 \text{ and } C_{2h}) \\ &> \text{Me}_2\text{Br}_4\,(C_{2h}) > \text{H}_4\text{Se}_2\text{Br}_6\,(C_i) \geq \text{Me}_4\text{Se}_2\text{Br}_6\,(C_i) \\ &\geq \mathbf{1}\,(C_i)_{\text{obsd}} > \mathbf{5}\,(C_i) > \mathbf{6}\,(C_i) > \text{Br}_6\,(C_{2h})_{\text{obsd}}, \end{aligned} \tag{10}$$

$$\begin{aligned} &\theta \text{ for } {}^{A}\text{Br} - * - {}^{B}\text{Br}: \\ &\text{H}_2\text{Br}_4\,(C_{2h}) > \text{Br}_6\,(C_{2h} \text{ and } C_2) \geq \text{Br}_6\,(C_{2h})_{\text{obsd}} \\ &> \text{Me}_2\text{Br}_4\,(C_{2h}) < \mathbf{1}\,(C_i)_{\text{obsd}} < \text{Me}_4\text{Se}_2\text{Br}_6\,(C_i) \\ &< \text{H}_4\text{Se}_2\text{Br}_6\,(C_i) < \mathbf{5}\,(C_i) \approx \mathbf{6}\,(C_i). \end{aligned} \tag{11}$$

Table 1: QTAIM functions and QTAIM-DFA parameters for ^{B}Br-∗-^{A}Br-∗-$^{A'}$Br-∗-$^{B'}$Br at BCPs in Br_4 σ(4c–6e), together with ^{A}Br-∗-^{A}Br in Br_2, evaluated with MP2/BSS-A[a].

Species (symmetry)	Interaction X-∗-Y	$\rho_b(\mathbf{r}_c)$ (ea_o^{-3})	$c\nabla^2\rho_b(\mathbf{r}_c)$[b] (au)	$H_b(\mathbf{r}_c)$ (au)	$k_b(\mathbf{r}_c)$[c]	R[d] (au)	θ[e] (°)	C_{ij} (Å mdyn^{-1})	$\theta_{p:CIV}$[f] (°)	$\kappa_{p:CIV}$[g] (au^{-1})	Predicted nature
Br_2 ($D_{\infty h}$)[h]	Br-∗-Br	0.1130	−0.0001	−0.0497	−2.005	0.0497	180.1	0.4	191.8	1.8	SS/Cov-w[i]
Br_4^{2-} ($D_{\infty h}$)[j]	^{A}Br-∗-^{A}Br	0.0922	0.0052	−0.0313	−1.751	0.0317	170.6	0.8	190.6	3.6	*r*-CS/CT-TBP[k]
	^{A}Br-∗-^{B}Br	0.0198	0.0058	0.0001	−0.995	0.0058	89.5	−19.6	118.2	146	*p*-CS/*t*-HB$_{nc}$[l]
Br_6 (C_2)	^{A}Br-∗-^{A}Br	0.1099	0.0010	−0.0466	−1.960	0.0467	178.8	0.4	191.3	2.3	*r*-CS/CT-TBP[k]
	^{A}Br-∗-^{B}Br	0.0131	0.0049	0.0009	−0.899	0.0050	79.6	14.3	97.8	105	*p*-CS/*t*-HB$_{nc}$[l]
Br_6 (C_{2h})[m]	^{A}Br-∗-^{A}Br	0.1099	0.0010	−0.0466	−1.961	0.0467	178.8	0.4	191.7	1.7	*r*-CS/CT-TBP[k]
	^{A}Br-∗-^{B}Br	0.0131	0.0049	0.0009	−0.899	0.0050	79.6	14.3	97.6	97	*p*-CS/*t*-HB$_{nc}$[l]
Br_6 (C_{2h})$_{obsd}$[n]	^{A}Br-∗-^{A}Br	0.0765	0.0053	−0.0200	−1.654	0.0207	165.2				*r*-CS
	^{A}Br-∗-^{B}Br	0.0156	0.0055	0.0007	−0.929	0.0055	82.5				*p*-CS
H_2Br_4 (C_{2h})	^{A}Br-∗-^{A}Br	0.1101	0.0008	−0.0468	−1.966	0.0468	179.0	0.4	191.7	2.0	*r*-CS/CT-TBP[k]
	^{A}Br-∗-^{B}Br	0.0118	0.0045	0.0010	−0.881	0.0046	78.0	15.5	94.7	100	*p*-CS/*t*-HB$_{nc}$[l]
Me_2Br_4	^{A}Br-∗-^{A}Br	0.1076	0.0016	−0.0444	−1.932	0.0445	177.9	0.4	191.4	1.8	*r*-CS/CT-TBP[k]
	^{A}Br-∗-^{B}Br	0.0164	0.0057	0.0006	−0.945	0.0057	84.1	10.5	105.1	100	*p*-CS/*t*-HB$_{nc}$[l]
$H_4Se_2Br_6$ (C_i)	^{A}Br-∗-^{A}Br	0.1028	0.0031	-0.0400	−1.866	0.0401	175.6	0.5	191.5	2.5	*r*-CS/CT-TBP[k]
	^{A}Br-∗-^{B}Br	0.0220	0.0068	−0.0002	−1.016	0.0068	91.9	9.9	117.4	75	*r*-CS/*t*-HB$_{wc}$[o]
$Me_4Se_2Br_6$ (C_i)	^{A}Br-∗-^{A}Br	0.1028	0.0032	−0.0400	−1.862	0.0402	175.4	0.5	191.4	3.7	*r*-CS/CT-TBP[k]
	^{A}Br-∗-^{B}Br	0.0212	0.0067	−0.0001	−1.008	0.0067	90.9	9.9	116.4	101	*r*-CS/*t*-HB$_{wc}$[o]
5 (C_i)[p]	^{A}Br-∗-^{A}Br	0.1016	0.0036	−0.0389	−1.844	0.0391	174.7	0.5	191.5	4.4	*r*-CS/CT-TBP[k]
	^{A}Br-∗-^{B}Br	0.0226	0.0070	−0.0003	−1.023	0.0070	92.7	6.8	118.0	557	*r*-CS/*t*-HB$_{wc}$[o]
	^{A}Br-∗-^{B}Br[q]	0.0226	0.0070	−0.0003	−1.023	0.0070	92.7	6.8	118.0	551	*r*-CS/*t*-HB$_{wc}$[o]
5 (C_i)[r]	^{A}Br-∗-^{A}Br	0.1047	0.0020	−0.0383	−1.905	0.0384	177.0	0.5	191.3	2.5	*r*-CS/CT-TBP[k]
	^{A}Br-∗-^{B}Br	0.0145	0.0048	0.0008	−0.904	0.0048	80.1	15.9	97.4	102	*p*-CS/*t*-HB$_{nc}$[o]
6 (C_i)	^{A}Br-∗-^{A}Br	0.1014	0.0037	−0.0388	−1.841	0.0389	174.6	0.5	191.5	36	*r*-CS/CT-TBP[k]
	^{A}Br-∗-^{A}Br[q]	0.1014	0.0037	−0.0388	−1.841	0.0389	174.6	0.5	191.6	36	*r*-CS/CT-TBP[k]
	^{A}Br-∗-^{B}Br[q]	0.0227	0.0070	−0.0004	−1.024	0.0071	92.8	42.1	122.5	2474	*r*-CS/*t*-HB$_{wc}$[o]
6 (C_i)[r]	^{A}Br-∗-^{A}Br	0.1044	0.0021	−0.0380	−1.901	0.0381	176.9	0.5	191.3	2.6	*r*-CS/CT-TBP[k]
	^{A}Br-∗-^{B}Br	0.0147	0.0048	0.0008	−0.907	0.0049	80.3	16.6	97.8	103	*p*-CS/*t*-HB$_{nc}$[o]
1 (C_i)[r]	^{A}Br-∗-^{A}Br	0.1063	0.0013	−0.0398	−1.939	0.0398	178.1	0.5	191.7	2.3	*r*-CS/CT-TBP[k]
	^{A}Br-∗-^{B}Br	0.0123	0.0043	0.0010	−0.868	0.0044	76.9	18.3	91.8	100	*p*-CS/*t*-HB$_{nc}$[l]
1 (C_i)$_{obsd}$[s]	^{A}Br-∗-^{A}Br	0.1019	0.0032	−0.0393	−1.860	0.0394	175.3				*r*-CS
	^{A}Br-∗-^{B}Br	0.0200	0.0066	0.0003	−0.979	0.0066	87.7				*p*-CS

[a]See the text for BSS. [b]$c\nabla^2\rho_b(\mathbf{r}_c) = H_b(\mathbf{r}_c) - V_b(\mathbf{r}_c)/2$, where $c = \hbar^2/8m$. [c]$k_b(\mathbf{r}_c) = V_b(\mathbf{r}_c)/G_b(\mathbf{r}_c)$. [d]$R = (x^2 + y^2)^{1/2}$, where $(x, y) = (H_b(\mathbf{r}_c) - V_b(\mathbf{r}_c)/2, H_b(\mathbf{r}_c))$. [e]$\theta = 90° - \tan^{-1}(y/x)$. [f]$\theta_p = 90° - \tan^{-1}(dy/dx)$. [g]$\kappa_p = |d^2y/dx^2|/[1 + (dy/dx)^2]^{3/2}$. [h]The Br-Br distance in Br_2 was optimized to be 2.2756 Å with MP2/BSS-A, which was very close to the observed distance in the gas phase (2.287 Å) [63]. However, the values are shorter than those determined by the X-ray crystallographic analysis (2.491 Å) [40] by 0.210 Å. The noncovalent Br---Br distance is 3.251 Å in crystal, which is shorter than the sum of the van der Waals radii [64] by 0.45 Å. [i]The SS interaction of the weak covalent nature. [j]With one imaginary frequency for the vibration mode of the SGU symmetry. [k]The *regular*-CS interaction of the CT-TBP nature. [l]The *pure*-CS interaction of the HB nature with no covalency. [m]With one imaginary frequency for the rotational mode around the linear Br_4 interaction. [n]See ref. [40] [o]The *regular*-CS interaction of the HB nature with covalency. [p]With one imaginary frequency for the vibration mode of the AU symmetry. [q]w = (0), ±0.025, and ±0.05. [r]At the CAM-B3LYP level. [s]See ref. [39].

Table 2: QTAIM functions and QTAIM-DFA parameters for ^{A}Br-∗-^{A}Se-∗-^{B}Br-∗-^{C}Br-∗-^{D}Br-∗-^{B}Se-∗-^{E}Br at BCPs in **7** (C_{2h}), **8** (C_{2h}), and **2** $(C_1)_{obsd}$, together with ^{A}Br-∗-^{A}Se-∗-^{B}Br in **3** (C_s) and ^{A}Br-∗-^{A}Se-∗-^{B}Br-∗-^{C}Br-∗-^{D}Br in **4** (C_s), evaluated with MP2 BSS-A[a)].

Species (symmetry)	Interaction X-∗-Y	$\rho_b(\mathbf{r}_c)$ (ea_o^{-3})	$c\nabla^2\rho_b(\mathbf{r}_c)$[b)] (au)	$H_b(\mathbf{r}_c)$ (au)	$k_b(\mathbf{r}_c)$[c)]	R[d)] (au)	θ[e)] (°)	C_{ij} (Å mdyn^{-1})	$\theta_{p:CIV}$[f)] (°)	$\kappa_{p:CIV}$[g)] (au^{-1})	Predicted nature
	^{A}Se-∗-^{A}Br[h)]	0.0423	0.0080	−0.0056	−1.258	0.0098	124.8	6.3	169.9	55	*r*-CS/CT-MC[i)]
7 (C_{2h})	^{A}Se-∗-^{B}Br[j)]	0.0825	0.0043	−0.0264	−1.753	0.0267	170.7	1.2	192.2	2.2	*r*-CS/CT-TBP[k)]
	^{B}Br-∗-^{C}Br[l)]	0.0335	0.0086	−0.0022	−1.115	0.0088	104.6	9.4	145.5	102	*r*-CS/*t*-HB$_{wc}$[m)]
	^{A}Se-∗-^{A}Br[h)]	0.0492	0.0085	−0.0079	−1.318	0.0116	133.0	2.3	172.7	53	*r*-CS/CT-MC[i)]
8 (C_{2h})	^{A}Se-∗-^{B}Br[j)]	0.0662	0.0075	−0.0158	−1.513	0.0175	154.6	2.2	187.7	17	*r*-CS/CT-TBP[k)]
	^{B}Br-∗-^{C}Br[l)]	0.0398	0.0092	−0.0038	−1.171	0.0100	112.5	4.2	151.5	54	*r*-CS/*t*-HB$_{wc}$[m)]
	^{A}Br-∗-^{A}Se	0.0219	0.0065	−0.0005	−1.039	0.0065	94.6				*r*-CS
	^{A}Se-∗-^{B}Br	0.0576	0.0102	−0.0113	−1.356	0.0152	137.8				*r*-CS
	^{B}Br-∗-^{C}Br	0.0952	0.0068	−0.0337	−1.713	0.0343	168.6				*r*-CS
2 $(C_1)_{obsd}$[n)]	^{C}Br-∗-^{D}Br	0.0183	0.0062	0.0005	−0.961	0.0062	85.7				*p*-CS
	^{D}Br-∗-^{B}Se	0.0818	0.0063	−0.0271	−1.682	0.0278	166.9				*r*-CS
	^{B}Se-∗-^{E}Br	0.0753	0.0072	−0.0220	−1.604	0.0231	161.9				*r*-CS
	^{A}Br-∗-^{A}Se	0.0737	0.0061	−0.0214	−1.636	0.0223	164.0	0.8	185.8	8.4	*r*-CS/CT-TBP[k)]
3 (C_s)	^{A}Se-∗-^{B}Br	0.0678	0.0069	−0.0177	−1.562	0.0189	158.7	1.0	183.0	18	*r*-CS/CT-TBP[k)]
	^{A}Br-∗-^{A}Se	0.0131	0.0042	0.0004	−0.945	0.0042	84.0	6.4	105.1	84	*p*-CS/*t*-HB$_{nc}$[o)]
4 (C_s)	^{A}Se-∗-^{B}Br	0.0425	0.0088	−0.0052	−1.229	0.0103	120.6	4.6	163.2	63	*r*-CS/CT-MC[i)]
	^{B}Br-∗-^{C}Br	0.0933	0.0059	−0.0321	−1.732	0.0326	169.6	0.9	192.1	5.6	*r*-CS/CT-TBP[k)]

[a)]See the text for BSS. [b)]$c\nabla^2\rho_b(\mathbf{r}_c) = H_b(\mathbf{r}_c) - V_b(\mathbf{r}_c)/2$, where $c = \hbar^2/8m$. [c)]$k_b(\mathbf{r}_c) = V_b(\mathbf{r}_c)/G_b(\mathbf{r}_c)$. [d)]$R = (x^2 + y^2)^{1/2}$, where $(x, y) = (H_b(\mathbf{r}_c) - V_b(\mathbf{r}_c)/2, H_b(\mathbf{r}_c))$. [e)]$\theta = 90° - \tan^{-1}(y/x)$. [f)]$\theta_p = 90° - \tan^{-1}(dy/dx)$. [g)]$\kappa_p = |d^2y/dx^2|/[1 + (dy/dx)^2]^{3/2}$. [h)]Because it has C_i symmetry, it is the same as ^{B}Se-∗-^{E}Br. [i)]The *regular*-CS interaction of the CT-MC nature. [j)]The same as ^{B}Se-∗-^{D}Br. [k)]The *regular*-CS interaction of the CT-TBP nature. [l)]The same as ^{C}Br-∗-^{D}Br. m) The *pure*-CS interaction of the HB nature with no covalency. [n)]See ref. [39]. [o)]The *regular*-CS interaction of the HB nature with no covalency.

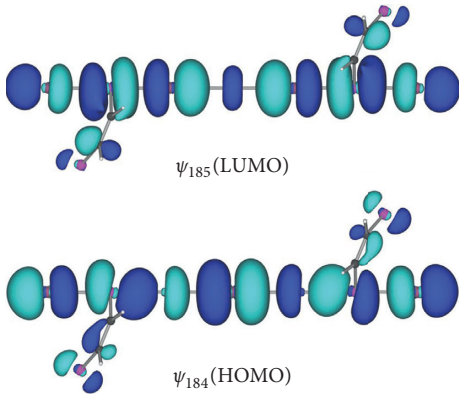

FIGURE 6: Molecular orbitals for σ(7c–10e). ψ_{184} (HOMO) and ψ_{185} (LUMO) of **8** (C_{2h}).

The orders shown in equations (10) and (11) seem to reasonably explain the characteristic behavior of Br_4 σ(4c–6e). The results must be the reflection of the $n_p(^{B}Br) \longrightarrow \sigma*(^{A}Br\text{-}^{A}Br) \leftarrow n_p(^{B}Br)$ form of Br_4 σ(4c–6e), where $^{A}Br\text{-}*\text{-}^{A}Br$ and $^{A}Br\text{-}*\text{-}^{B}Br$ become weaker and stronger, respectively, as the CT interaction increases. Br_4 σ(4c–6e) will be stabilized more effectively, if the negative charge is developed more at ^{B}Br. However, the two Br^- ligands in Br_4^{2-} ($D_{\infty h}$) seem not so effective than that expected. This would come from the electrostatic repulsive factor between the double negative charges in Br_4^{2-} ($D_{\infty h}$), as mentioned above.

The θ values for ($^{A}Br\text{-}*\text{-}^{A}Br$ and $^{A}Br\text{-}*\text{-}^{B}Br$) in Br_6 $(C_{2h})_{obsd}$ and **1** $(C_i)_{obsd}$ are (165.2°, 82.5°) and (175.3°, 87.7°), respectively. Therefore, $^{A}Br\text{-}*\text{-}^{A}Br$ and $^{A}Br\text{-}*\text{-}^{B}Br$ are classified by *r*-CS and *p*-CS, respectively. Both $^{A}Br\text{-}*\text{-}^{A}Br$ and $^{A}Br\text{-}*\text{-}^{B}Br$ in Br_6 $(C_{2h})_{obsd}$ are predicted to be weaker than those in **1** $(C_i)_{obsd}$, respectively. The results would be curious at the first glance, since $^{A}Br\text{-}*\text{-}^{A}Br$ will be weaker, if $^{A}Br\text{-}*\text{-}^{B}Br$ in $^{B}Br\text{-}*\text{-}^{A}Br\text{-}*\text{-}^{A}Br\text{-}*\text{-}^{B}Br$ becomes stronger, as mentioned above. They would be affected from the surrounding, such as the crystal packing effect. A Br_2 molecule interacts with four bromine atoms adjacent to the Br_2 molecule on the *bc*-plane in crystals, equivalently with 3.251 Å [40].

Similar investigations were carried out for I_4 σ(4c–6e), which will be discussed elsewhere (it is demonstrated that Br_4 σ(4c–6e) is predicted to be somewhat stronger than I_4 σ(4c–6e)).

3.6. Nature of Se_2Br_5 σ(7c–10e). The nature of Se_2Br_5 σ(7c–10e) in **7** (C_{2h}) and **8** (C_{2h}) is elucidated, together with $SeBr_2$ σ(3c–4e) in **3** and $SeBr_4$ σ(4c–6e) in **4**. The results are collected in Table 2. Figure 6 shows symmetric ψ_{184} (HOMO) and antisymmetric ψ_{185} (LUMO) of **8** (C_{2h}), which correspond to ψ_5 and ψ_6 in σ(7c–10e), illustrated in Figure 1 although the Se atoms are contained in the linear Se_2Br_5 σ(7c–10e) in **8** (C_{2h}). The linear seven atomic orbitals on Se_2Br_5 are shown to construct ψ_{184} (HOMO) and ψ_{185} (LUMO) of **8** (C_{2h}), which can be analysed as the Se_2Br_5 σ(7c–10e) [39], so can the linear interaction in **7** (C_{2h}), although not shown. The pseudolinear interaction of the seven atoms of **1** $(C_1)_{obsd}$ could also be explained by the Se_2Br_5 σ(7c–10e) model.

The results demonstrate that Se_2Br_5 σ(7c–10e) stabilize well **7** (C_{2h}) and **8** (C_{2h}) although **1** $(C_1)_{obsd}$ seems not so effective. The negative charge developed at the Br atom in **3** would not be sufficient to stabilize Se_2Br_5 σ(7c–10e) in **1** $(C_1)_{obsd}$, relative to the case of the Br^- anion in **7** (C_{2h}) and **8** (C_{2h}), irrespective of the highly negatively charged Br atoms in $SeBr_2$ σ(3c–4e) of **3**.

4. Conclusion

The intrinsic dynamic and static nature of Br_4 σ(4c–6e) is elucidated for **1** $(C_i)_{obsd}$ and the related species with QTAIM-DFA, employing the perturbed structures generated with CIV. The $^{A}Br\text{-}^{A}Br$ interactions in $^{B}Br\text{-}*\text{-}^{A}Br\text{-}*\text{-}^{A}Br\text{-}*\text{-}^{B}Br$ of Br_4 σ(4c–6e) are weaker than Br-*-Br in the optimized structure of Br_2 ($D_{\infty h}$), which is predicted to have the SS/Cov-w nature. The $^{A}Br\text{-}^{A}Br$ interactions in Br_4 σ(4c–6e) of the models are predicted to have the *r*-CS/CT-TBP nature, if optimized with MP2/BSS-A. The $^{A}Br\text{-}^{A}Br$ interaction in **1** $(C_i)_{obsd}$ also appears in the *r*-CS region. On the contrary, the $^{A}Br\text{-}^{B}Br$ interactions in Br_6 (C_2), Br_6 (C_{2h}), H_2Br_4 (C_{2h}), and Me_2Br_4 (C_{2h}) are predicted to have the *p*-CS/*t*-HB_{nc} nature, whereas those in $H_4Se_2Br_4$ (C_i), $Me_4Se_2Br_4$ (C_i), **5** (C_i), and **6** (C_i) have the *r*-CS/*t*-HB_{wc} nature, if evaluated with MP2/BSS-A. The $^{A}Br\text{-}*\text{-}^{B}Br$ interactions become stronger in the order of H_2Br_4 (C_{2h}) < Br_6 (C_{2h}) ≤ Br_6 (C_2) < Me_2Br_4 (C_{2h}) << $Me_4Se_2Br_6$ (C_i) ≤ $H_4Se_2Br_6$ (C_i) ≤ **5** (C_i) < **6** (C_i), which is the inverse order for $^{A}Br\text{-}*\text{-}^{A}Br$, as a whole. The results are in accordance with the CT interaction of the $n_p(^{B}Br) \longrightarrow \sigma*(^{A}Br\text{-}^{A}Br) \leftarrow n_p(^{B}Br)$ form derived from Br_4 σ(4c–6e). The decreased binding force of $^{A}Br\text{-}*\text{-}^{A}Br$ must be transferred to $^{A}Br\text{-}*\text{-}^{B}Br$ in Br_4 σ(4c–6e). Namely, it is demonstrated that Br_4 σ(4c–6e) is stabilized as the strength of $^{A}Br\text{-}*\text{-}^{B}Br$ in Br_4 σ(4c–6e) increases, while $^{A}Br\text{-}*\text{-}^{A}Br$ becomes weakened relative to that in the original Br_2 ($D_{\infty h}$). In this process, Br_4 σ(4c–6e) is totally stabilized. The $^{A}Br\text{-}*\text{-}^{A}Br$ and $^{A}Br\text{-}*\text{-}^{B}Br$ interactions in Br_6 $(C_{2h})_{obsd}$ and **1** $(C_i)_{obsd}$ are classified by the *r*-CS and *p*-CS interactions, respectively, where the interactions in Br_6 $(C_{2h})_{obsd}$ seem somewhat weaker than those in **1** $(C_i)_{obsd}$. The Se_2Br_5 σ(7c–10e) interactions are similarly elucidated for **2** $(C_1)_{obsd}$ and the anionic models of **7** (C_{2h}) and **8** (C_{2h}). The Se_2Br_5 σ(7c–10e) nature is clearly established for the optimized structures of **7** (C_{2h}) and **8** (C_{2h}), rather than **2** $(C_1)_{obsd}$. Extended hypervalent interactions of the $\sigma(mc\text{–}ne$: $4 \le m$; $m < n < 2m)$ type are shown to be well analysed and evaluated with QTAIM-DFA, employing the perturbed structures generated with CIV, exemplified by Br_4 σ(4c–6e) and Se_2Br_5 σ(7c–10e).

Data Availability

The data used to support the findings of this study are available in the supplementary information files.

Conflicts of Interest

The authors declare that there are no conflicts of interest regarding the publication of this paper.

Acknowledgments

This work was partially supported by a Grant-in-Aid for Scientific Research (no. 17K05785) from the Ministry of Education, Culture, Sports, Science, and Technology of Japan.

Supplementary Materials

Scheme S1: classification of interactions by the signs of $\nabla^2\rho_b(\mathbf{r}_c)$ and $H_b(\mathbf{r}_c)$, together with $G_b(\mathbf{r}_c)$ and $V_b(\mathbf{r}_c)$. Scheme S2: QTAIM-DFA: a plot of $H_b(\mathbf{r}_c)$ versus $H_b(\mathbf{r}_c) - V_b(\mathbf{r}_c)/2$ for weak to strong interactions. Scheme S3: rough classification and characterization of interactions by θ and θ_p, together with $k_b(\mathbf{r}_c)$ (= $V_b(\mathbf{r}_c)/G_b(\mathbf{r}_c)$). QTAIM-DFA approach, computational data (Tables S2–S5 and Figures S3–S5), computation information and geometries of compounds, and graphical abstract. Figure S1: polar (R, θ) coordinate representation of $H_b(\mathbf{r}_c)$ versus $H_b(\mathbf{r}_c) - V_b(\mathbf{r}_c)/2$, with ($\theta_p$, κ_p) parameters. Figure S2: plot of $H_b(\mathbf{r}_c)$ versus w in $r(^1\text{Cl-}^2\text{Cl}) = r_o(^1\text{Cl-}^2\text{Cl}) + wa_o$ for $^1\text{Cl-}^2\text{Cl-}^3\text{Cl}^-$ (a) with the magnified picture of (a) (b) and that of $H_b(\mathbf{r}_c) - V_b(\mathbf{r}_c)/2$ versus w (c). Typical hydrogen bonds without covalency and typical hydrogen bonds with covalency are abbreviated as *t*-HB without cov. and *t*-HB with cov., respectively, whereas Cov-w and Cov-s stand for weak covalent bonds and strong covalent bonds, respectively. Table S1: proposed definitions for the classification and characterization of interactions. (*Supplementary Materials*)

References

[1] G. C. Pimentel, "The bonding of trihalide and bifluoride ions by the molecular orbital method," *The Journal of Chemical Physics*, vol. 19, no. 4, pp. 446–448, 1951.

[2] J. I. Musher, "The chemistry of hypervalent molecules," *Angewandte Chemie International Edition in English*, vol. 8, no. 1, pp. 54–68, 1969.

[3] K.-Y. Akiba, *Chemistry of Hypervalent Compounds*, Wiley-VCH, New York, USA, 1999.

[4] A. J. Mukherjee, S. S. Zade, H. B. Singh, and R. B. Sunoj, "Organoselenium chemistry: role of intramolecular interactions†," *Chemical Reviews*, vol. 110, no. 7, pp. 4357–4416, 2010.

[5] S. Patai and Z. Rappoport, *The Chemistry of Organic Selenium and Tellurium Compounds*, Vol. 1, Wiley, New York, USA, 1986.

[6] J. C. Martin and M. M. Chau, "Anchimerically accelerated bond homolysis. VII: simultaneous participation of three neighboring groups in the transition state for a radical-forming perester decomposition: new route to hypervalent compounds of sulfur and iodine," *Journal of the American Chemical Society*, vol. 96, no. 10, pp. 3319–3321, 1974.

[7] W. Nakanishi, S. Hayashi, and T. Arai, "Linear alignment of four sulfur atoms in bis[(8-phenylthio)naphthyl] disulfide: contribution of linear S4 hypervalent four-centre six-electron bond to the structure," *Chemical Communications*, vol. 2002, no. 20, pp. 2416-2417, 2002.

[8] W. Nakanishi, S. Hayashi, S. Morinaka, T. Sasamori, and N. Tokitoh, "Extended hypervalent E′---E-E---E′ 4c-6e (E, E′ = Se, S) interactions: structure, stability and reactivity of 1-(8-PhE′C10H6)EE(C10H6E′Ph-8′)-1′," *New Journal of Chemistry*, vol. 32, no. 11, pp. 1881–1889, 2008.

[9] W. Nakanishi, S. Hayashi, and S. Toyota, "Four-center six-electron interaction versus lone Pair–Lone pair interaction between selenium atoms in naphthalene peri positions," *The Journal of Organic Chemistry*, vol. 63, no. 24, pp. 8790–8800, 1998.

[10] W. Nakanishi, "Hypervalent chalcogen compounds (chapter 10.3)," in *Handbook of Chalcogen Chemistry: New Perspectives in Sulfur, Selenium and Tellurium*, F. A. Devillanova, Ed., Royal Society of Chemistry, London, UK, pp. 644–668, 2006.

[11] W. Nakanishi and S. Hayashi, "Hypervalent chalcogen compounds (chapter 12.3)," in *Handbook of Chalcogen Chemistry: New Perspectives in Sulfur, Selenium and Tellurium*, F. A. Devillanova and W.-W. du Mont, Eds., vol. 2pp. 335–372, Royal Society of Chemistry, Cambridge, UK, 2nd edition, 2013.

[12] W. Nakanishi, S. Hayashi, M. Hashimoto, M. Arca, M. C. Aragoni, and V. Lippolis, *The Chemistry of Organic Selenium and Tellurium Compounds*, Z. Rappoport, Ed., vol. 4, pp. 885–972, Wiley, New York, USA, 2014.

[13] W. Nakanishi, S. Hayashi, and N. Itoh, "Extended hypervalent 5c–6e interactions: linear alignment of five C–Se---O---Se–C atoms in anthraquinone and 9-methoxyanthracene bearing arylselanyl groups at the 1,8-positions," *The Journal of Organic Chemistry*, vol. 69, no. 5, pp. 1676–1684, 2004.

[14] A. Panda, G. Mugesh, H. B. Singh, and R. Butcher, "Synthesis, structure, and reactivity of organochalcogen (Se, Te) compounds derived from 1-(N,N-Dimethylamino)naphthalene and N,N-dimethylbenzylamine," *Organometallics*, vol. 18, no. 10, pp. 1986–1993, 1999.

[15] M. Kulcsar, A. Beleaga, C. Silvestru et al., "Solid state structure and solution behaviour of organoselenium(ii) compounds containing 2-{E(CH_2CH_2)2NCH_2}C_6H_4 groups (E = O, NMe)," *Dalton Transactions*, vol. 2007, no. 21, pp. 2187–2196, 2007.

[16] M. C. Durrant, "A quantitative definition of hypervalency," *Chemical Science*, vol. 6, no. 11, pp. 6614–6623, 2015.

[17] M. S. Schmøkel, S. Cenedese, J. Overgaard et al., "Testing the concept of hypervalency: charge density analysis of K_2SO_4," *Inorganic Chemistry*, vol. 51, no. 15, pp. 8607–8616, 2012.

[18] Z. Rappoport, *The Chemistry of Organic Selenium and Tellurium Compounds*, vol. 4, pp. 989–1236, Wiley, New York, USA, 2014.

[19] P. Kilian, F. R. Knight, and J. D. Woollins, "Naphthalene and related systemsperi-substituted by group 15 and 16 elements," *Chemistry—A European Journal*, vol. 17, no. 8, pp. 2302–2328, 2011.

[20] R.-F. Hu, Y.-H. Wen, J. Zhang, Z.-J. Li, and Y.-G. Yao, "4,4′-bipyridylium bis(hydrogen 2,2′-dithiodibenzoate) dihydrate," *Acta Crystallographica Section E Structure Reports Online*, vol. 60, no. 11, pp. o2029–o2031, 2004.

[21] S. Wang, H. Mao-Lin, and F. Chen, "catena-Poly[[[aqua-zinc(II)]-μ-2,2′-dithiodibenzoato] bis(N,N-dimethylformamide)]," *Acta Crystallographica Section E Structure Reports Online*, vol. 60, no. 4, pp. m413–m415, 2004.

[22] X.-J. Wang, Z.-F. Chen, B.-S. Kang et al., "Chemistry of 2-mercaptophenol (H2mp) . Part iii. One dimensional arrays of binuclear anions of Mo (VI) linked by bis (2-hydroxyphenyl) disulfide via hydrogen bondings," *Polyhedron*, vol. 18, no. 5, pp. 647–655, 1999.

[23] T. Mak, W. Yip, W. Chan, G. Smith, and C. Kennard, "The crystal structure of bis(2-chlorophenyl) disulfide," *Australian Journal of Chemistry*, vol. 42, no. 8, pp. 1403–1406, 1989.

[24] Y. Tsubomoto, S. Hayashi, and W. Nakanishi, "Dynamic and static behavior of the E-E′ bonds (E, E′ = S and Se) in cystine and derivatives, elucidated by AIM dual functional analysis," *RSC Advances*, vol. 5, no. 15, pp. 11534–11540, 2015.

[25] W. Nakanishi, Y. Tsubomoto, and S. Hayashi, "Nature of S2Se2 σ(4c-6e) at naphthalene 1,8-positions and models, elucidated by QTAIM dual functional analysis," *RSC Advances*, vol. 6, no. 95, pp. 93195–93204, 2016.

[26] S. Hayashi, Y. Tsubomoto, and W. Nakanishi, "Behavior of the E-E' bonds (E, E' = S and Se) in glutathione disulfide and derivatives elucidated by quantum chemical calculations with the quantum theory of atoms-in-molecules approach," *Molecules*, vol. 23, no. 2, pp. 443–451, 2018.

[27] Y. Tsubomoto, S. Hayashi, W. Nakanishi, L. K. Mapp, and S. J. Coles, "High-resolution X-ray diffraction determination of the electron density of 1-(8-PhSC10H6)SS(C10H6SPh-8′)-1′ with the QTAIM approach: evidence for S4 σ(4c-6e) at the naphthalene peri-positions," *RSC Advances*, vol. 8, no. 18, pp. 9651–9660, 2018.

[28] R. F. W. Bader, *Atoms in Molecules. A Quantum Theory*, Oxford University Press, Oxford, UK, 1990.

[29] C. F. Matta and R. J. Boyd, *An Introduction to the Quantum Theory of Atoms in Molecules in the Quantum Theory of Atoms in Molecules: From Solid State to DNA and Drug Design*, Wiley-VCH, Weinheim, Germany, 2007.

[30] F. Biegler-König and J. Schönbohm, "Update of the AIM2000-program for atoms in molecules," *Journal of Computational Chemistry*, vol. 23, no. 15, pp. 1489–1494, 2002.

[31] F. Biegler-König, J. Schönbohm, and D. Bayles, "Software news and updates, AIM2000—a program to analyze and visualize atoms in molecules," *Journal of Computational Chemistry*, vol. 22, no. 5, pp. 545–559, 2001.

[32] R. F. W. Bader, "A bond path: a universal indicator of bonded interactions," *The Journal of Physical Chemistry A*, vol. 102, no. 37, pp. 7314–7323, 1998.

[33] R. F. W. Bader, "A quantum theory of molecular structure and its applications," *Chemical Reviews*, vol. 91, no. 5, pp. 893–928, 1991.

[34] R. F. W. Bader, "Atoms in molecules," *Accounts of Chemical Research*, vol. 18, no. 1, pp. 9–15, 1985.

[35] T. H. Tang, R. F. W. Bader, and P. J. MacDougall, "Structure and bonding in sulfur-nitrogen compounds," *Inorganic Chemistry*, vol. 24, no. 13, pp. 2047–2053, 1985.

[36] R. F. W. Bader, T. S. Slee, D. Cremer, and E. Kraka, "Description of conjugation and hyperconjugation in terms of electron distributions," *Journal of the American Chemical Society*, vol. 105, no. 15, pp. 5061–5068, 1983.

[37] F. W. Biegler-könig, R. F. W. Bader, and T.-H. Tang, "Calculation of the average properties of atoms in molecules II," *Journal of Computational Chemistry*, vol. 3, no. 3, pp. 317–328, 1982.

[38] Y. Tsubomoto, S. Hayashi, W. Nakanishi, T. Sasamori, and N. Tokitoh, "Nature of $E_2X_2\sigma$(4c-6e) of the *X*---*E*-*E*---*X* type at naphthalene 1,8-positions and model, elucidated by X-ray crystallographic analysis and QC calculations with the QTAIM approach," *Acta Crystallographica Section B Structural Science, Crystal Engineering and Materials*, vol. 73, no. 2, pp. 265–275, 2017.

[39] W. Nakanishi, S. Hayashi, S. Yamaguchi, and K. Tamao, "First Br_4 four centre-six electron and Se_2Br_5 seven centre-ten electron bonds in nonionic bromine adducts of selenanthrene," *Chemical Communications*, vol. 2004, no. 2, pp. 140-141, 2004.

[40] B. M. Powell, K. M. Heal, and B. H. Torrie, "The temperature dependence of the crystal structures of the solid halogens, bromine and chlorine," *Molecular Physics*, vol. 53, no. 4, pp. 929–939, 1984.

[41] H. Vogt, D. Wulff-Molder, and M. Meisel, "Synthese und kristallstruktur der (p-brombenzyl)triphenylphosphoniumbromide: $[(p\text{-}Br\text{-}C_6H_4\text{-}CH_2)P(C_6H_5)_3]^+B^-$;$[(p\text{-}Br\text{-}C_6H_4\text{-}CH_2)P(C_6H_5)^3]^+Br^{2-}$ und $[(p\text{-}Br\text{-}C_6H_4\text{-}CH_2)P(C_6H_5)_3]^+Br^{3-}$," *Zeitschrift für Naturforschung B*, vol. 51, no. 10, pp. 1443–1448, 1996.

[42] W. Nakanishi, S. Hayashi, and K. Narahara, "Polar coordinate representation of $h_b(\mathbf{r}_c)$ versus $(\hbar^2/8m)\nabla^2\rho_b(\mathbf{r}_c)$ at BCP in AIM analysis: classification and evaluation of weak to strong interactions," *The Journal of Physical Chemistry A*, vol. 113, no. 37, pp. 10050–10057, 2009.

[43] W. Nakanishi, S. Hayashi, and K. Narahara, "Atoms-in-molecules dual parameter analysis of weak to strong interactions: behaviors of electronic energy densities versus laplacian of electron densities at bond critical points," *The Journal of Physical Chemistry A*, vol. 112, no. 51, pp. 13593–13599, 2008.

[44] W. Nakanishi and S. Hayashi, "Atoms-in-Molecules dual functional analysis of weak to strong interactions," *Current Organic Chemistry*, vol. 14, no. 2, pp. 181–197, 2010.

[45] W. Nakanishi and S. Hayashi, "Dynamic behaviors of interactions: application of normal coordinates of internal vibrations to AIM dual functional analysis," *The Journal of Physical Chemistry A*, vol. 114, no. 27, pp. 7423–7430, 2010.

[46] W. Nakanishi, S. Hayashi, K. Matsuiwa, and M. Kitamoto, "Applications of normal coordinates of internal vibrations to generate perturbed structures: dynamic behavior of weak to strong interactions elucidated by atoms-in-molecules dual functional analysis," *Bulletin of the Chemical Society of Japan*, vol. 85, no. 12, pp. 1293–1305, 2012.

[47] W. Nakanishi and S. Hayashi, "Role of dG/dw and dV/dw in AIM analysis: an approach to the nature of weak to strong interactions," *The Journal of Physical Chemistry A*, vol. 117, no. 8, pp. 1795–1803, 2013.

[48] W. Nakanishi and S. Hayashi, "Perturbed structures generated using coordinates derived from compliance constants in internal vibrations for QTAIM dual functional analysis: intrinsic dynamic nature of interactions," *International Journal of Quantum Chemistry*, vol. 118, no. 11, Article ID e25590, 2018.

[49] K. Brandhorst and J. Grunenberg, "Efficient computation of compliance matrices in redundant internal coordinates from Cartesian Hessians for nonstationary points," *The Journal of Chemical Physics*, vol. 132, no. 18, Article ID 184101, 2010.

[50] K. Brandhorst and J. Grunenberg, "How strong is it? The interpretation of force and compliance constants as bond strength descriptors," *Chemical Society Reviews*, vol. 37, no. 8, pp. 1558–1567, 2008.

[51] J. Grunenberg, "III-defined concepts in chemistry: rigid force constants *vs.* compliance constants as bond strength descriptors for the triple bond in diboryne," *Chemical Science*, vol. 6, no. 7, pp. 4086–4088, 2015.

[52] The Unit of C_{ij} is Å $mdyn^{-1}$, $Å^3$ $Mdyn^{-1}$ in Reference 50 Should Read Å $mdyn^{-1}$.

[53] S. Hayashi, T. Nishide, and W. Nakanishi, "Behavior of multi-HBs in acetic acid dimer and related species: QTAIM dual functional analysis employing perturbed structures generated using coordinates from compliance force constants," *Bulletin of the Chemical Society of Japan*, vol. 92, no. 1, pp. 87–96, 2019.

[54] M. J. Frisch, G. W. Trucks, H. B. Schlegel et al., *Gaussian 09 (Revision D.01)*, Gaussian, Inc., Wallingford, CT, USA, 2009.
[55] T. Noro, M. Sekiya, and T. Koga, "Segmented contracted basis sets for atoms H through Xe: Sapporo-(DK)-*n*ZP sets (*n* = D, T, Q)," *Theoretical Chemistry Accounts*, vol. 131, no. 2, pp. 1124–1131, 2012.
[56] C. Møller and M. S. Plesset, "Note on an approximation treatment for many-electron systems," *Physical Review*, vol. 46, no. 7, pp. 618–622, 1934.
[57] J. Gauss, "Effects of electron correlation in the calculation of nuclear magnetic resonance chemical shifts," *The Journal of Chemical Physics*, vol. 99, no. 5, pp. 3629–3643, 1993.
[58] J. Gauss, "Accurate calculation of NMR chemical shifts," *Berichte der Bunsengesellschaft für physikalische Chemie*, vol. 99, no. 8, pp. 1001–1008, 1995.
[59] Y. Zhao and D. G. Truhlar, "The M06 suite of density functionals for main group thermochemistry, thermochemical kinetics, noncovalent interactions, excited states, and transition elements: two new functionals and systematic testing of four M06-class functionals and 12 other functionals," *Theoretical Chemistry Accounts*, vol. 120, no. 1–3, pp. 215–241, 2008.
[60] F. Biegler-König, "Calculation of atomic integration data," *Journal of Computational Chemistry*, vol. 21, no. 12, pp. 1040–1048, 2000.
[61] T. A. Keith, *AIMAll (Version 17.11.14)*, TK Gristmill Software, Overland Park, KS, USA, 2017, http://aim.tkgristmill.com/.
[62] E. D. GlendeningJ. K. Badenhoop et al., *Theoretical Chemistry Institute*, University of Wisconsin, Madison, WI, USA, 2013.
[63] Y. Iwasawa, Ed.*Kagakubinran Kisohen II*, Maruzen, Tokyo, Japan, 5th edition, 2004.
[64] A. Bondi, "van der Waals volumes and radii," *The Journal of Physical Chemistry*, vol. 68, no. 3, pp. 441–451, 1964.